Title

Potential of Depth-of-Interaction-Based Detection Time Correction in Cherenkov Emitter Crystals for TOF-PET

Journal

IEEE Transactions on Radiation and Plasma Medical Sciences, 7(3)

ISSN

2469-7311

Authors

He, Xuzhi

Trigila, Carlotta

Ariño-Estrada, Gerard

et al.

Publication Date

2023-03-01

DOI

10.1109/trpms.2022.3226950

Peer reviewed

HHS Public Access

Author manuscript

IEEE Trans Radiat Plasma Med Sci. Author manuscript; available in PMC 2024 March 01.

Published in final edited form as:

IEEE Trans Radiat Plasma Med Sci. 2023 March ; 7(3): 233–240. doi:10.1109/trpms.2022.3226950.

Potential of Depth-of-Interaction-Based Detection Time Correction in Cherenkov Emitter Crystals for TOF-PET

Xuzhi He [Member, IEEE],
Department of Biomedical Engineering at the University of California Davis, Davis, CA 95616 USA.

Carlotta Trigila [Member, IEEE],
Department of Biomedical Engineering at the University of California Davis, Davis, CA 95616 USA.

Gerard Ariño-Estrada [Member, IEEE],
Department of Biomedical Engineering at the University of California Davis, Davis, CA 95616 USA.

Emilie Roncali [Senior Member, IEEE]
Department of Biomedical Engineering at the University of California Davis, Davis, CA 95616 USA.

Department of Radiology at University of California Davis, Sacramento, CA 95817 USA

Abstract

Cherenkov light can improve the timing resolution of Positron Emission Tomography (PET) radiation detectors, thanks to its prompt emission. Coincidence time resolutions (CTR) of ~30 ps were recently reported when using 3.2 mm-thick Cherenkov emitters. However, sufficient detection efficiency requires thicker crystals, causing the timing resolution to be degraded by the optical propagation inside the crystal. We report on depth-of-interaction (DOI) correction to mitigate the time-jitter due to the photon time spread in Cherenkov-based radiation detectors. We simulated the Cherenkov and scintillation light generation and propagation in 3×3 mm^2 lead fluoride, lutetium oxyorthosilicate, bismuth germanate, thallium chloride, and thallium bromide. Crystal thicknesses varied from 9 to 18 mm with a 3-mm step. A DOI-based time correction showed a 2-to-2.5-fold reduction of the photon time spread across all materials and thicknesses. Results showed that highly refractive crystals, though producing more Cherenkov photons, were limited by an experimentally obtained high-cutoff wavelength and refractive index, restricting the propagation and extraction of Cherenkov photons mainly emitted at shorter wavelengths. Correcting the detection time using DOI information shows a high potential to mitigate the photon time spread. These simulations highlight the complexity of Cherenkov-based detectors and the competing factors in improving timing resolution.

eroncali@ucdavis.edu.

This work did not involve human subjects or animals in its research.

Keywords

PET; Cherenkov; timing resolution; depth-of-interaction; photon transport; radiation detectors; simulation

I. INTRODUCTION

The goal of engineering gamma detectors with 10 ps time resolution is driving the development of detector instrumentation for time-of-flight positron emission tomography (TOF-PET) [1] using prompt photons emitted at least an order of magnitude faster than current scintillation photons [2]. Cherenkov light generated after the interaction of a 511 keV gamma-ray with the detector material [3] is an attractive alternative to scintillation light thanks to its picosecond emission. Benchtop detector setups based on Cherenkov emitters with 3.2 mm thickness (e.g., bismuth germanate) and microchannel plate photomultipliers (MCP-PMTs) have shown time resolutions of 27 ps full width at half maximum (FWHM) [4] [5], demonstrating the potential of prompt photons. Such values were achieved thanks to the excellent transition time spread of MCP-PMTs and minimal photon time spread in such a short crystal combined with deep learning to estimate the timing information [6] [7]. Many simulation and experimental studies have shown how photon time spread increases with the crystal thickness due to greater variation of the depth-of-interaction (DOI), number of reflections, light loss, and subsequently of the light transport until it becomes the dominating factor in time resolution [8] [9] [10] [11]. Although photon time spread affects Cherenkov and scintillation photons differently due to their different emission angular distribution (Fig. 1) the magnitude of the effect is similar. Any DOI correction methods developed to fully exploit the potential of Cherenkov photons will also benefit other prompt photons and scintillation photons. Other groups have pursued analytical modeling and empirical correction of the DOI to improve timing resolution [12] [13].

We used Monte Carlo simulations to study the mitigation of the photon time spread with DOI information in Cherenkov emitters in 9 mm to 18 mm-thick crystals with dual-ended readout. The crystals used are summarized in Table 1. While benchtop detector experiments routinely provide access to coincidence timing resolution, measuring photon time spread alone is not trivial due to the combination of light transport, light extraction, photodetector response, and finite timing resolution of frontend readout electronics. Particle and optical simulations where parameters can be controlled and monitored individually are well suited to estimate small variations of time distributions in different configurations, as well as to disentangle the effect of DOI segmentation and DOI resolution. We selected four materials previously studied as Cherenkov emitters for TOF-PET lead fluoride (PbF_2), bismuth germanate (BGO), thallium chloride (TlCl), and thallium bromide (TlBr) [14] [8] [15] [16] [17]. The choice of these different materials was guided by their refractive indices leading to different Cherenkov yields, specific cut-off wavelengths and absorption properties, and scintillation yields. Additionally, lutetium oxyorthosilicate (LSO) was included, as it is the crystal choice in commercial TOF-PET detectors [18]. Table 1 summarizes the physical properties of these five materials. TlCl and TlBr are promising semiconductors for Cherenkov charge induction (CCI) detectors that combine good energy, DOI resolution,

and spatial resolution. In previous work [19], we used experiments and simulations to demonstrate the potential of these materials to produce detectable Cherenkov signals that are not smeared by the presence of scintillation. Two factors related to the DOI were evaluated in this work: the DOI resolution, reflecting the detector precision in measuring the DOI position, and the DOI binning used to sort out interactions by their DOI. We investigated the possible reduction of photon time spread with a DOI-based correction of optical photon time stamps, modeling the DOI information with a DOI resolution of 0.75 mm or 2.5 mm. A 2.5 mm-DOI resolution is representative of current dual-ended detectors with 20 mm-thick LSO and BGO crystals [20], while a 0.75 mm DOI resolution assesses the usefulness of a very fine DOI encoding to improve time accuracy.

We simulated the effect of the photodetector photodetection efficiency (PDE) for all materials and dimensions, modeling state-of-the-art silicon photomultipliers (Hamamatsu S14160-3050) [19] or ideal detectors with a PDE of 1. Practical implementation of such DOI-encoding or photodetector PDE is only briefly mentioned in the discussion and is not the primary focus of this work.

II. Materials and Methods

A. GATE Simulation

1) Materials and Detector Configuration—Monoenergetic 511 keV back-to-back gamma photon interactions and optical photon transport were simulated in GATE v9.0 [21] for LSO, PbF_2, BGO, TlCl and TlBr. For each material, four crystals with a 3×3 mm^2 cross-section and a thickness of 9, 12, 15, or 18 mm were modeled. All surfaces were modeled as polished and air-coupled with Teflon [22] [23] except for the two 3×3 mm^2 faces, which were modeled coupled to a photodetector through a thin layer of optical grease (0.1 mm, index of refraction of 1.47). The optical grease was assumed to have a 100% transparency for Cherenkov photons. The source activity was set to 30,000 Bq, with an isotropic emission to collect a total of 9000–19000 photoelectric events in the detector, depending on the configuration and material. Compton events were not considered, as they are typically excluded from coincidence timing resolution studies. The optical photons produced by scintillation and Cerenkov emission from energetic electrons were simultaneously generated using the Livermore Model [24].

2) Optical Modelling—The optical properties of each material were modeled through the index of refraction, cut-off wavelength, and absorption length (e.g. 13 and 2.5 cm for BGO between 320 nm and 800 nm), which all depend on the wavelength (Table 1, Fig. 2). Note that PbF_2 and TlBr do not scintillate and only produce Cerenkov photons, as opposed to the other materials. The crystal surfaces and optical reflections were described with the LUT Davis model [25] and custom LUTs computed for each material [26]. The reflectance of the different materials is shown in Fig. 2. We considered the wavelength ranging from cut-off to 800 nm. Only visible photons with a wavelength between the cutoff wavelength and 800 nm were considered in the analysis (Table 1, Fig. 2). The cut-off wavelength and the index of refraction combined play an important role in determining what fraction of the Cherenkov emitted photons can propagate in the crystal, cross the exit face to ultimately

reach the photodetector and be counted as detected (Fig. 2). For example, PbF_2 has a low cutoff at 250 nm and a low index of refraction of ~1.75 at 500 nm, while TlBr has a much higher cut-off at 440 nm and a higher index of refraction > 2.5. The lower detection yield resulting from these optical properties counteracts the higher Cherenkov production yield of high index materials predicted by the Frank-Tamm equation [3]. The generation of Cherenkov photons along the tracks of electrons emitted by the interaction of the 511 keV gamma with the crystal was processed by Geant4 using the electron momentum and index of refraction of the medium. The number of generated Cherenkov photons depends on the electron step length, which was parameterized in Geant4 through the maximum allowed kinetic energy change at each step based on previous studies [27]. The electron trajectory also affects the Cherenkov photon emission direction and path to the photodetector [3]. The number of emitted scintillation photons is determined by the material scintillation yield and energy of the incident gamma photon. Scintillation photons were emitted isotropically with time stamps following an exponential decay corresponding to the know decay times of the materials. Scintillation rise times were not included in the study.

For each detected optical photon, the wavelength, transit time in the crystal, and arrival time at the photodetector sensitive area were recorded (Fig. 1). The transit time was measured from the gamma interaction time in the crystal and did not include the gamma transit time. Gamma photons travel at the speed of light c in vacuum, while optical photons travel at the speed of light in the crystal c/n, making the index of refraction a critical parameter to the photon transport. To allow the comparison of detection time patterns between gamma events, the detection time of each optical photon was defined as the difference between its unique arrival time and the gamma transit time. The electron transit time is negligible and was not included.

B. DOI Modelling

Events were classified as “front” or “back” based on the first optical photon detection side (front or back photodetector, respectively, Fig. 1). To model a realistic uncertainty on the events position identification, a Gaussian blurring was applied to the DOI of individual events with a resolution of 0.75 mm or 2.5 mm FWHM. The resolution was chosen based on DOI resolution values we previously measured with benchtop similar detectors [28] [20].

C. DOI Correction

The performance of the DOI correction was evaluated for an ideal case (no DOI blurring) and for two DOI resolutions (0.75 mm and 2.5 mm). Each of these scenarios was explored for two DOI bin widths (1 mm and 3 mm). The relationship between the DOI and event detection time was studied for each material and each photodetector. Fig. 3 shows the example of a 12 mm-thick crystal with a DOI blurring of 2.5 mm and events sorted into four DOI bins of 3 mm width. To correct for the DOI time walk, an offset corresponding to the minimum time required to travel from the center of the DOI bin to the photodetector was applied to individual event detection times. The offset depends on the optical photon speed in the crystal, which was considered independent of the wavelength in this case and defined as the nominal refractive index for each material. For each DOI bin and each detector side, the detection times were histogrammed, as shown in Fig. 3 top left for the front

photodetector. The DOI histograms of corrected detection times show a good alignment at 0 ps (Fig. 3, top right and bottom right).

D. Evaluation of Photon Time Spread

For a given DOI bin, the photon time spread is determined by the emission position, emission time, and transit time (Fig. 1) and strongly affects the detector timing resolution. We evaluated the photon time spread through the width of the detection time distributions after correcting for the DOI walk. The sum of all DOI histograms was fitted with a Gaussian distribution to compute the FWHM (Fig. 3), which was used as a proxy for the photon time spread. The contribution of the optical transit time in the crystal to the detection time was also evaluated by histogramming the transit times in each DOI bin.

III. Results

A. Photon Transit Time

Fig. 4 show the distribution of optical transit times recorded by the front photodetector for each 3 mm DOI bin in a 12 mm thick BGO crystal for Cherenkov and scintillation photons separately. Cherenkov and scintillation photons exhibit similar behaviors with a primary peak corresponding to photons directed towards the photodetector and a secondary peak of much lower amplitude (see inset in Fig. 4, both left and bottom) corresponding to photons reflected in the back of the crystal before getting recorded by the photodetector. In the case of this 12 mm thick BGO crystal, the secondary peaks are between ~150 ps and ~220 ps.

B. Event Detection Times

Fig. 5 shows scatter plots of event detection times before DOI-time correction as a function of the DOI for Cherenkov and scintillation times (red and blue points, respectively). PbF_2 and TlBr show no scintillation events because they do not scintillate. To illustrate the DOI effect, results are shown for 18 mm thick crystals, without DOI blurring. In all five materials, the Cherenkov detection times showed a linear relationship with the DOI from 0 to 18 mm, while the scintillation photon detection times were more scattered due to greater variation in light yield, emission time, and emission direction combined. Note that only detection times lower than 300 ps are shown on these plots and that scintillation detection times extend beyond this limit in some configurations. LSO shows the greatest density of scintillation events close to the Cherenkov region due to its fast decay time of 40 ns and high scintillation light (~35000 photons/MeV). It also has the clearest separation between front and back photodetectors: most events generated in the first half of the crystal between 0 and 9 mm were detected by the front photodetector, while most events generated in the second half between 9 mm and 18 mm were detected by the closest photodetector at the backside. In contrast, the slow decay time of BGO (~300 ns) and its low light yield of 8500 photons/MeV explains the sparse distribution of scintillation detection times. TlCl shows a greater density of scintillation events than BGO despite a lower scintillation light yield (~2000 photons/MeV), thanks to its much faster decay time of 10 ns. Longer detection times visible with TlBr around 300 ps corresponded to photons reflected on the other side of the crystal before detection, as illustrated in Fig. 4. With values between 2.7 and 2.35 between 440 nm and 800 nm, TlBr has the highest index of refraction, 2.7, among all five materials

and thus has the highest index mismatch between the exit face and the coupling medium to the photodetector. This increases the reflection of optical photons on the exit face instead of favoring their extraction, resulting in more photons reflected by the opposite face. These curves could also provide a continuous DOI correction method.

The detection times (combination of scintillation and Cherenkov photons and scintillation is added if it is emitted) were corrected for DOI time walk in each bin as illustrated in Fig. 3 and histogrammed after correction.

Fig. 6 shows the distributions for a DOI blurring of 2.5 mm, 1 mm, and 3 mm DOI binning, for back and front detection times combined. The distributions of the uncorrected detection times (in red) were flat and wide, while the DOI correction yielded much narrower detection time histograms that were well fitted with a Gaussian distribution (R^2 >0.95 for all ideal PDE distributions, and R^2>0.86 such as 0.89, 0.9, 0.93, 0.95, 0.96, 0.97, 0.98, for real PDE distributions). The FWHM of the Gaussian fit applied to the entire histogram, was used to characterize the photon time spread of each configuration. Distributions of other crystal thicknesses are shown in supplementary data (Fig. S1, Fig. S2, Fig. S3).

C) Photon time spread characterized from detection time distributions

Fig. 7 summarizes the FWHM of the detection time distributions for all scenarios and for back and front detectors combined: no DOI blurring (0 mm), blurring of 0.75 mm and 2.5 mm, ideal and real photodetector PDE, DOI binning of 1 mm and 3 mm. As explained above, all distributions were corrected for the DOI time walk. Fig. S4 shows the results for Cerenkov photons only.

1) Effect of DOI blurring and DOI binning—Considering all materials, as shown in Fig. 7, adding a DOI blurring of 0.75 mm did not change the width of the detected time distributions, while a DOI blurring of 2.5 mm increased the FWHM. The effect was stronger for the 1 mm bin (square markers in Fig. 7), which could be expected with a blurring wider than the bin size, as more events got assigned to the incorrect DOI bin and were corrected with the incorrect DOI time walk. The DOI blurring of 2.5 mm decreased the effect of other factors, such as bin size and PDE, as indicated by the smaller distance between the curves.

For all materials and all crystal thicknesses, reducing the bin size decreased the FWHM. Thicker crystals (18 mm) had the largest FWHM, indicating a greater variation in detection time. In these crystals, the transport time (Fig. 4) increased with the DOI and became the dominant factor in the detection time, especially for Cherenkov photons whose emission time is within 10 ps.

2) Effect of PDE—Modeling the PDE of the photodetector adds a random deletion of optical photons reaching the photodetector face, increasing the uncertainty on the first detected photon for each event and subsequently broadening the detection time distributions (larger FWHM shown as blue marker in Fig. 7). The LSO FWHM increased from 25.29 ps to 32.42 ps (increase around 28%) at 18 mm for a DOI binning of 3 mm, while for TlCl an increase from 35.05 ps to 48.34 ps (increase around 38%) was observed at 18 mm (Fig.

7, bottom row, DOI resolution=2.5 mm). LSO and BGO, of which scintillation emission spectra match well the PDE spectrum (Fig. 2), were less affected by SiPM performance.

3) Comparison of materials—PbF_2 only emits Cherenkov and showed the lowest photon time spread between 10 ps and 25 ps. When considering all photons, PbF_2 and LSO showed comparable performance, although LSO detection times are a combination of fast Cherenkov and slow scintillation photons. Interestingly, TlCl and TlBr, which have higher refractive indices and produce more Cherenkov photons per gamma interaction in the crystal, showed poorer performance, especially for 3 mm bins. We studied the FWHM of the Cherenkov photons separately.

Fig. 5 shows that only the bins in the crystal half closest to the photodetector contributed to detection times for both Cherenkov and scintillation photons for LSO. In contrast, TlBr and TlCl showed a contribution much more uniform across the DOI. This translated into much broader event detection time distributions, explaining the differences in FWHM reported in Fig. 7.

4) Cherenkov vs. scintillation photons—When considering only Cherenkov photons in LSO (not shown), the FWHM further decreased (e.g., from 32 ps to 25 ps at 18 mm with a 3 mm bin, 2.5 mm DOI resolution, and real PDE), indicating that the larger number of photons collected through scintillation (i.e., greater statistics) does not reduce the distribution width and photon time spread. Only LSO showed an improvement in FWHM when eliminating the scintillation; no significant difference was observed in BGO or TlCl.

IV. Discussion

We studied the relation between the optical photon time spread and the depth-of-interaction in five materials used as gamma radiation detectors. We studied different components of the photon time spread separately: crystal thickness, photodetector PDE, DOI resolution and DOI binning. To characterize the photon time spread, we studied the event detection time distributions and extracted their FWHM, which accounts for the DOI blurring, binning, optical transport, and photodetector model. The event detection times were taken as the first detected photon, which could be a Cherenkov or scintillation photon.

Among DOI resolution and DOI segmentation, the largest of the two limits the potential of correction of photon time spread. For simulations with 2.5 mm DOI blurring (equivalent to a 2.5 mm DOI resolution, representative of state-of-the-art pixelated detectors) [20], the difference between 1 mm and 3 mm segmentation is very modest (Fig. 7, bottom row). Simulations with no blurring or with a 0.75 mm DOI blurring (Fig. 7, top and middle rows) give very similar results and suggest the segmentation is limiting the correction in this scenario. Therefore, using a DOI segmentation matching the DOI resolution would provide the most efficient correction for DOI time walk and ultimately improve the timing resolution.

For each scenario of DOI segmentation and DOI resolution, there were minor variations in the FWHM outcome among the type of material, photodetector PDE, and crystal thickness.

The photodetector PDE only becomes relevant for the scenarios with thicker crystals with higher refractive indices such as TlCl. It is also worth noting that for the worst scenario, an 18 mm thick TlBr, PDE=50%, DOI resolution of 2.5 mm and DOI binning of 3 mm, the photon time spread is 50 ps, which remains below the SPTR of state-of-the-art silicon photomultipliers [29]. High frequency readout electronics with high power consumption plays an essential role to achieve excellent SPTR as well. Fig. 7 summarizes the photon time spread as characterized by the FWHM of the detection time distributions for all photons. It shows that materials with a higher index of refraction exhibit a larger photon time spread, although their greater Cherenkov production was expected to result in a lower time spread. This is due to the combined effect of the cut-off wavelength and lower extraction efficiency at the exit face. These results suggest that to become competitive, TlCl and TlBr would require optimized coupling interfaces to maximize the light extraction and capture by the photodetector, such as photonic crystals. Thanks to their semi-conductor properties, these materials are attractive to build pixelated CCI detectors that can offer a fine DOI-resolution with either a single or dual-ended readout detector [30]. Better detection time resolution will be obtained thanks to the improvement in DOI resolution.

The simulations presented in this paper will also be used in the future to evaluate the ratio of photons detected by the front and the back detectors and optimize the use of a dual-ended readout scheme. The dual-ended readout configurations presented here typically provide a robust DOI estimation [20] and increase the photon detection efficiency compared to single-ended photodetector coupling. However, other approaches could be taken. Single-ended DOI-based estimation in scintillation crystals have been proposed by used of phosphor coating [31], stacked layers [32], high-frequency readout [33], DOI-encoded light sharing [34]. This study focused on using a dual-ended readout scheme, following or previous experimental work and with the goal of investigating the optimization of Cerenkov photon collection. Although the Cerenkov emission exhibits some directionality it remains weak, thus their collection might be improved by using a dual-ended readout geometry.

V. Conclusion

We have studied the potential of correcting the detection time in Cherenkov emitters using DOI information. The process shows a high potential to mitigate the photon time spread of Cherenkov and scintillation photons, especially in longer crystals and materials with a high index of refraction. The accuracy of the DOI estimation plays a very significant role in the correction and might motivate future efforts to build benchtop systems with simultaneous high time and DOI estimation accuracy. By providing a detailed picture of the optical transport and detection in radiation detectors, these simulations also highlight the complexity of Cherenkov-based detectors and the competing factors in improving timing resolution.

Supplementary Material

Refer to Web version on PubMed Central for supplementary material.

Acknowledgements

All authors declare that they have no known conflicts of interest in terms of competing financial interests or personal relationships that could have an influence or are relevant to the work reported in this paper. This work has been funded by NIH awards R01 EB027130 and R01 EB029533.

References

[1]. Nemallapudi MV, Gundacker S, Lecoq P, Auffray E, Ferri A, Gola A and Piemonte C, “Sub-100 ps coincidence time resolution for positron emission tomography with LSO:Ce codoped with Ca,” Physics in Medicine and Biology, vol. 60, pp. 4635–49, 2015. [PubMed: 26020610]

[2]. Lecoq P et al. , “Roadmap toward the 10 ps time-of-flight PET challenge,” Physics in medicine and biology, vol. 65, no. 1361–6560, p. 21RM01, 2020.

[3]. Jelley JV, “Cerenkov radiation and its applications,” Br. J. Appl. Phys, vol. 6, pp. 227—232, 1955.

[4]. Kwon SI, Ota R, Berg E, Hashimoto F, Nakajima K, Ogawa I, Tamagawa Y, Omura T, Hasegawa T and Cherry SR, “Ultrafast timing enables reconstruction-free positron emission imaging,” Nature Photonics, vol. 15, pp. 914–918, 2021. [PubMed: 35663419]

[5]. Ota R, Nakajima K, Ogawa I, Tamagawa Y, Shimoi H, Suyama M and Hasegawa T, “Coincidence time resolution of 30 ps FWHM using a pair of Cherenkov-radiator-integrated MCP-PMTs,” Physics in Medicine and Biology, vol. 64, p. 07LT01, 2019.

[6]. Berg E and Cherry SR, “Using convolutional neural networks to estimate time-of-flight from PET detector waveforms,” Physics in Medicine and Biology, vol. 63, no. 2, p. 02LT01, 2018.

[7]. Ota R et al. , “Lead-free MCP to improve coincidence time resolution and reduce MCP direct interactions,” Physics in Medicine and Biology, vol. 66, no. 6, p. 064006, 2021. [PubMed: 33636710]

[8]. Kratochwil N, Gundacker S, Lecoq P and Auffray E, “Pushing Cherenkov PET with BGO via coincidence time resolution classification and correction,” Physics in Medicine and Biology, vol. 65, p. 115004, 2020. [PubMed: 32268304]

[9]. WW M, WS C and SE D, “MODELING TIME DISPERSION DUE TO OPTICAL PATH LENGTH DIFFERENCES IN SCINTILLATION DETECTORS,” Acta Phys Pol B Proc Suppl, vol. 7, pp. 725–734, 2014. [PubMed: 25729464]

[10]. Moses W and Derenzo S, “Prospects for time-of-flight PET using LSO scintillator,” IEEE Transactions on Nuclear Science, vol. 46, pp. 474–478, 1999.

[11]. Roncali E, Il Kwon S, Jan S, Berg E and Cherry SR, “Cerenkov light transport in scintillation crystals explained: realistic simulation with GATE,” Biomedical Physics and Engineering Express, vol. 5, p. 035033, 2019. [PubMed: 33304614]

[12]. Efthimiou N et al. , “TOF-PET Image Reconstruction With Multiple Timing Kernels Applied on Cherenkov Radiation in BGO,” IEEE Transactions on Radiation and Plasma Medical Sciences, vol. 5, no. 5, pp. 703–711, 2021.

[13]. Kratochwil N, Auffray E and Gundacker S, “Exploring Cherenkov Emission of BGO for TOF-PET,” IEEE Transactions on Radiation and Plasma Medical Sciences, vol. 5, no. 5, pp. 619–629, 2021.

[14]. Ariño-Estrada G, Mitchell GS, Kwon SI, Du J, Kim H, Cirignano LJ, Shah KS and Cherry SR, “Towards time-of-flight PET with a semiconductor detector,” Physics in Medicine and Biology, vol. 63, p. 04LT01, 2018.

[15]. Kratochwil N, Gundacker S and Auffray E, “A roadmap for sole Cherenkov radiators with SiPMs in TOF-PET,” Physics in Medicine and Biology, vol. 66, p. 195001, 2021.

[16]. Kwon SI, Roncali E, Gola A, Paternoster G, Piemonte C and Cherry SR, “Dual-ended readout of bismuth germanate to improve timing resolution in time-of-flight PET,” Physics in Medicine and Biology, vol. 64, p. 105007, 2019. [PubMed: 30978713]

[17]. Terragni G, Pizzichemi M, Roncali E, Cherry SR, Glodo J, Shah K, Ariño-Estrada G, Auffray E, Ghezzi A and Kratochwil N, “Time Resolution Studies of Thallium Based Cherenkov Semiconductors,” Frontiers in Physics, vol. 10, 2022.

[18]. van Sluis J, de Jong J, Schaar J, Noordzij W, van Snick P, Dierckx R, Borra R, Willemsen A and Boellaard R, “Performance characteristics and quantitative clinical evaluation of the digital Siemens Biograph Vision PET/CT,” Journal of Nuclear Medicine, vol. 60, p. 109, 2019.

[19]. Ariño-Estrada G et al. , “Study of Čerenkov Light Emission in the Semiconductors TlBr and TlCl for TOF-PET,” IEEE Transactions on Radiation and Plasma Medical Sciences, vol. 5, no. 5, pp. 630–637, 2021. [PubMed: 34485785]

[20]. Junwei D, Gerard A-E, Xiaowei B and C. S. R, “Performance comparison of dual-ended readout depth-encoding PET detectors based on BGO and LYSO crystals,” Physics in Medicine and Biology, vol. 65, p. 235030, 2020.

[21]. Sarrut D et al. , “Advanced Monte Carlo simulations of emission tomography imaging systems with GATE,” Physics in Medicine and Biology, vol. 66, 2021.

[22]. Trigila C and Roncali E, “Integration of polarization in the LUTDavis model for optical Monte Carlo simulation in radiation detectors,” Physics in Medicine and Biology, vol. 66, no. 21, 2021.

[23]. Roncali E, Stockhoff M and Cherry SR, “An integrated model of scintillator-reflector properties for advanced simulations of optical transport,” Physics in Medicine and Biology, vol. 62, no. 1361–6560, pp. 4811–4830, 2017. [PubMed: 28398905]

[24]. Apostolakis J et al. , “Adaptive track scheduling to optimize concurrency and vectorization in GeantV,” Journal of Physics: Conference Series, vol. 608, p. 012003, 2015.

[25]. Stockhoff M, Jan S, Dubois A, Cherry SR and Roncali E, “Advanced optical simulation of scintillation detectors in GATE V8.0: first implementation of a reflectance model based on measured data,” Physics in Medicine and Biology, vol. 62, pp. L1–L8, 2017. [PubMed: 28452339]

[26]. Trigila C, Moghe E and Roncali E, “Technical Note: Standalone application to generate custom reflectance Look-Up Table for advanced optical Monte Carlo simulation in GATE/Geant4,” Medical Physics, vol. 48, pp. 2800–2808, 2021. [PubMed: 33772816]

[27]. Trigila C, Ariño-Estrada G, Il KS and Roncali E, “The Accuracy of Cerenkov Photons Simulation in Geant4/Gate Depends on the Parameterization of Primary Electron Propagation,” Frontiers in Physics, vol. 10, 2022.

[28]. Ariño-Estrada G, Du J, Kim H, Cirignano LJ, Shah KS, Cherry SR and Mitchell GS, “Development of TlBr detectors for PET imaging,” Physics in Medicine and Biology, vol. 63, p. 13NT04, 2018.

[29]. Gundacker S, Martinez Turtos R, Kratochwil N, Pots RH, Paganoni M, Lecoq P and Auffray E, “Experimental time resolution limits of modern SiPMs and TOF-PET detectors exploring different scintillators and Cherenkov emission,” Physics in Medicine and Biology, vol. 65, p. 025001, 2020.

[30]. Ariño-Estrada G, Kim H, Du J, Cirignano LJ, Shah KS and Cherry SR, “Energy and electron drift time measurements in a pixel CCI TlBr detector with 1.3 MeV prompt-gammas,” Physics in Medicine and Biology, vol. 66, p. 044001, 2021. [PubMed: 33326951]

[31]. Roncali E, Viswanath V and Cherry SR, “Design Considerations for DOI-encoding PET Detectors Using Phosphor-Coated Crystals,” IEEE Transactions on Nuclear Science, vol. 61, pp. 67–73, 2014.

[32]. Hong S, Yang J and Kang J, “A DOI-PET detector inserting glass plates to provide multiple spatial resolutions,” Nuclear Instruments and Methods in Physics Research Section A: Accelerators, Spectrometers, Detectors and Associated Equipment, vol. 1020, p. 165903, 2021.

[33]. Loignon-Houle F, Gundacker S, Toussaint M, Camirand Lemyre F, Auffray E, Fontaine R, Charlebois SA, Lecoq P and Lecomte R, “DOI estimation through signal arrival time distribution: a theoretical description including proof of concept measurements,” Physics in Medicine and Biology, vol. 66, 2021.

[34]. LaBella A, Cao X, Petersen E, Lubinsky R, Biegon A, Zhao W and Goldan AH, “High-Resolution Depth-Encoding PET Detector Module with Prismatoid Light-Guide Array,” Journal of Nuclear Medicine, vol. 61, pp. 1528–1533, 2020. [PubMed: 32111684]

[35]. Trigila C and Roncali E, “Effect of crystal-photodetector interface extraction efficiency on Cerenkov photons’ detection time,” Frontiers in Physics, vol. 10, 2022.

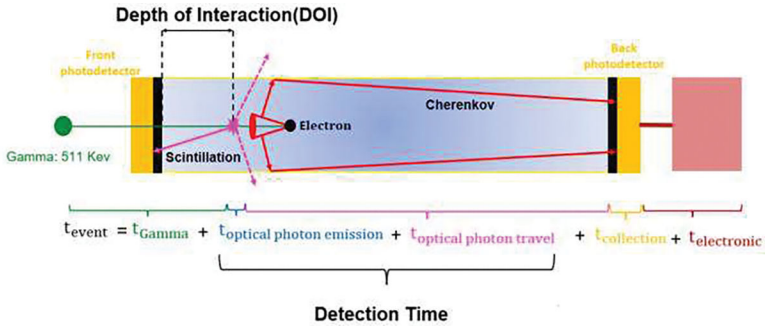

Fig. 1.

Simulation setup: A monoenergetic 511 KeV gamma source was placed in front of the detector. Interactions within the scintillator generated optical photons (scintillation or Cherenkov) that were tracked until they were detected or lost through the crystal sides. Both 3×3 mm^2 faces were modeled coupled to a photodetector (front and back, respectively); all other faces were modeled coupled with Teflon through a thin air layer. The scintillator thickness was varied from 9 mm, 12 mm, 15 mm, and 18 mm.

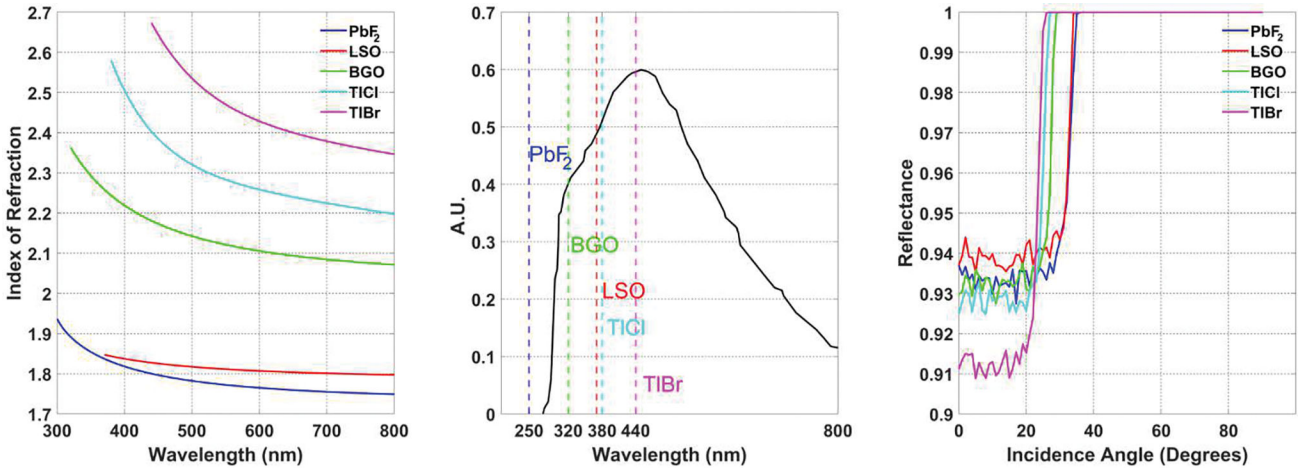

Fig. 2.

Material optical properties. Left: Index of refraction as a function of wavelength. Middle: Emission spectra and SiPM PDE (black). The vertical lines indicate the transmission cut-off wavelength. Right: Reflectance probability as a function of incidence angle for all materials showing the different critical angles. We considered the wavelength ranging from cut-off to 800 nm.

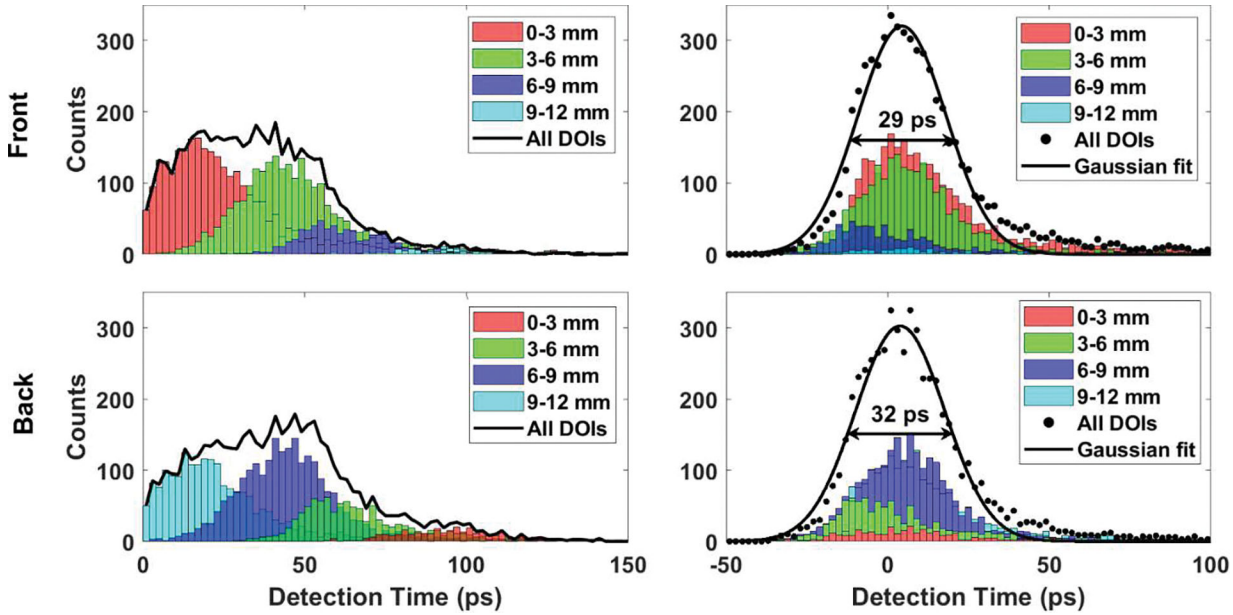

Fig. 3.

DOI-correction. Top: Photon detection time distribution at the front photodetector before and after DOI correction. Bottom: Photon detection time distribution at the back photodetector before and after DOI correction (farther from the entrance face). The summed photon detection time distributions for all DOIs are shown in black, with a Gaussian fit applied (solid curve). The fits had a FWHM of 29 ps and 32 ps for the front and back photodetectors, respectively.

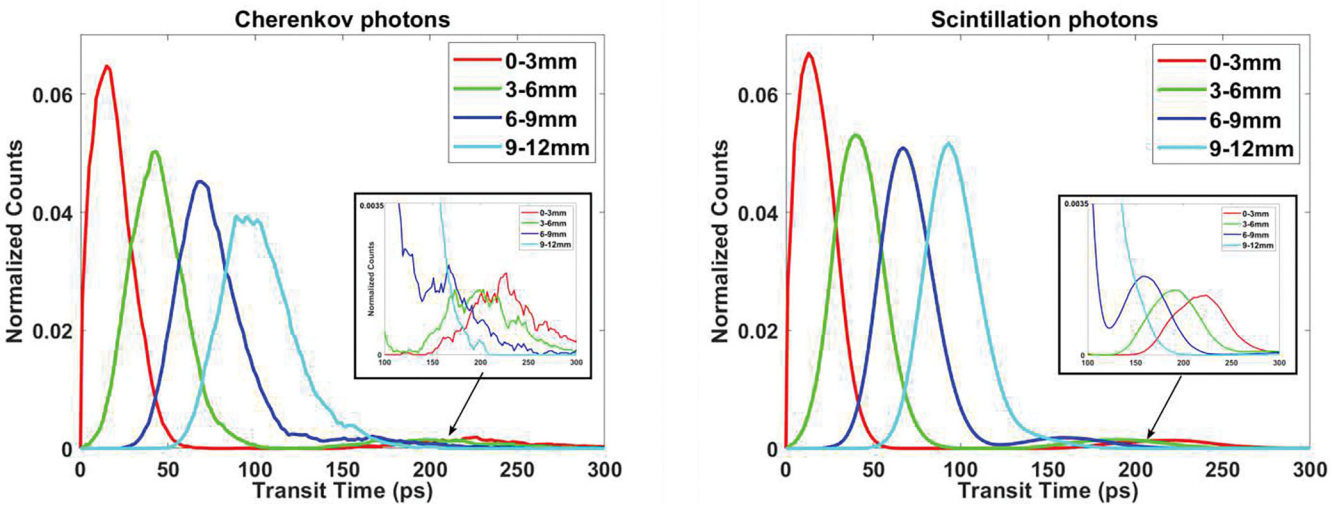

Fig. 4.

Optical transport in a 12 mm thick BGO crystal wrapped with Teflon. Top: Cherenkov photons. Bottom: Scintillation photons. Histograms of transit times values for all detected photons emitted at different DOIs and collected by the front detector show that both photon types exhibit similar transit time distributions, with a primary early peak followed by a delayed peak corresponding to photons reflected on the other side of the crystal before detection.

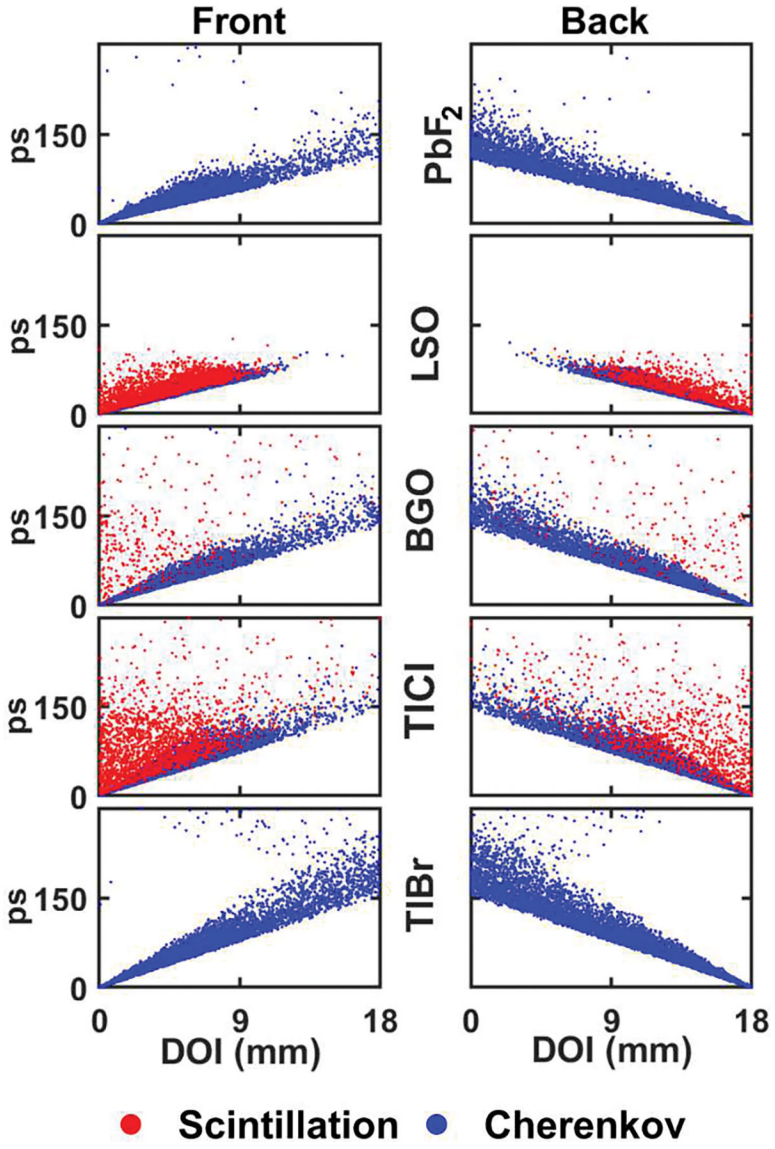

Fig. 5.

Event detection times as a function of DOI for LSO, PbF_2, BGO, TlCl, and TlBr. DOI resolution is 0 mm. All crystals were 3 × 3 × 18 mm^3. Left: Front photodetector. Right: Back photodetector.

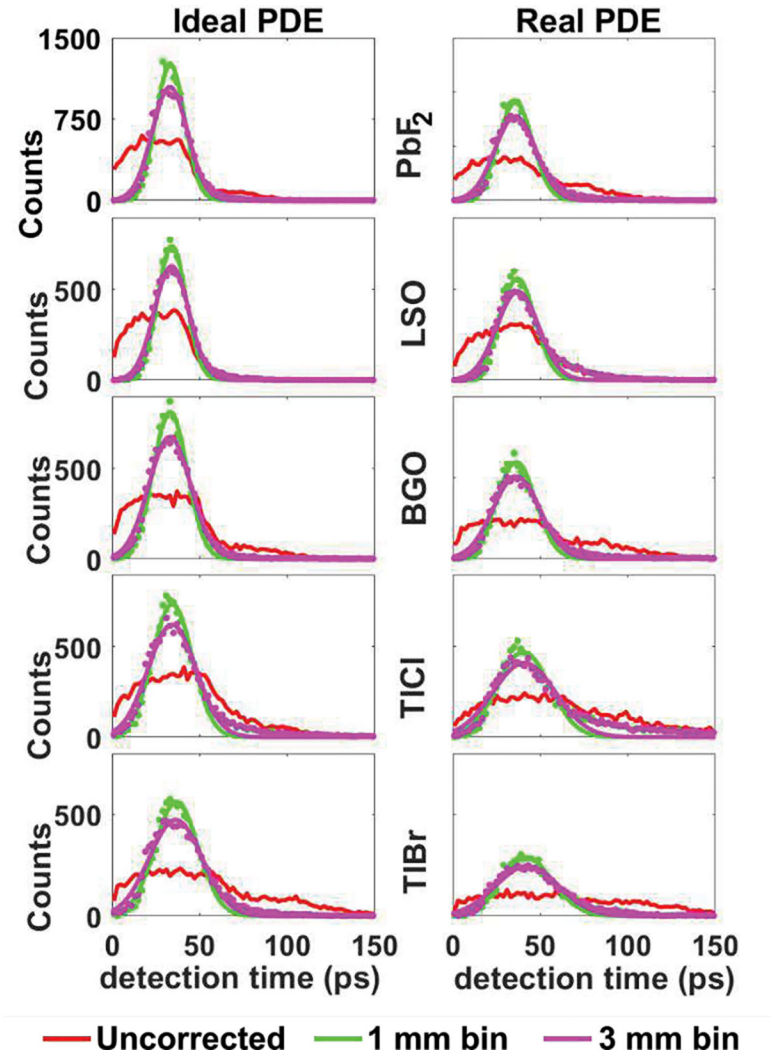

Fig. 6.

Detection time distributions for a 2.5 mm DOI blurring and different DOI binning (1mm and 3 mm) in 12 mm thick crystals. Distributions before DOI correction (in red) are wide and flat. For both 1 mm and 3 mm binning the DOI correction reduced the width of the curves and allowed for a Gaussian fit to be applied. In the case of a real PDE modeling, random deletion of detection time at the photodetector level increased the uncertainty in the detection time distribution, which is shown by noisier curves.

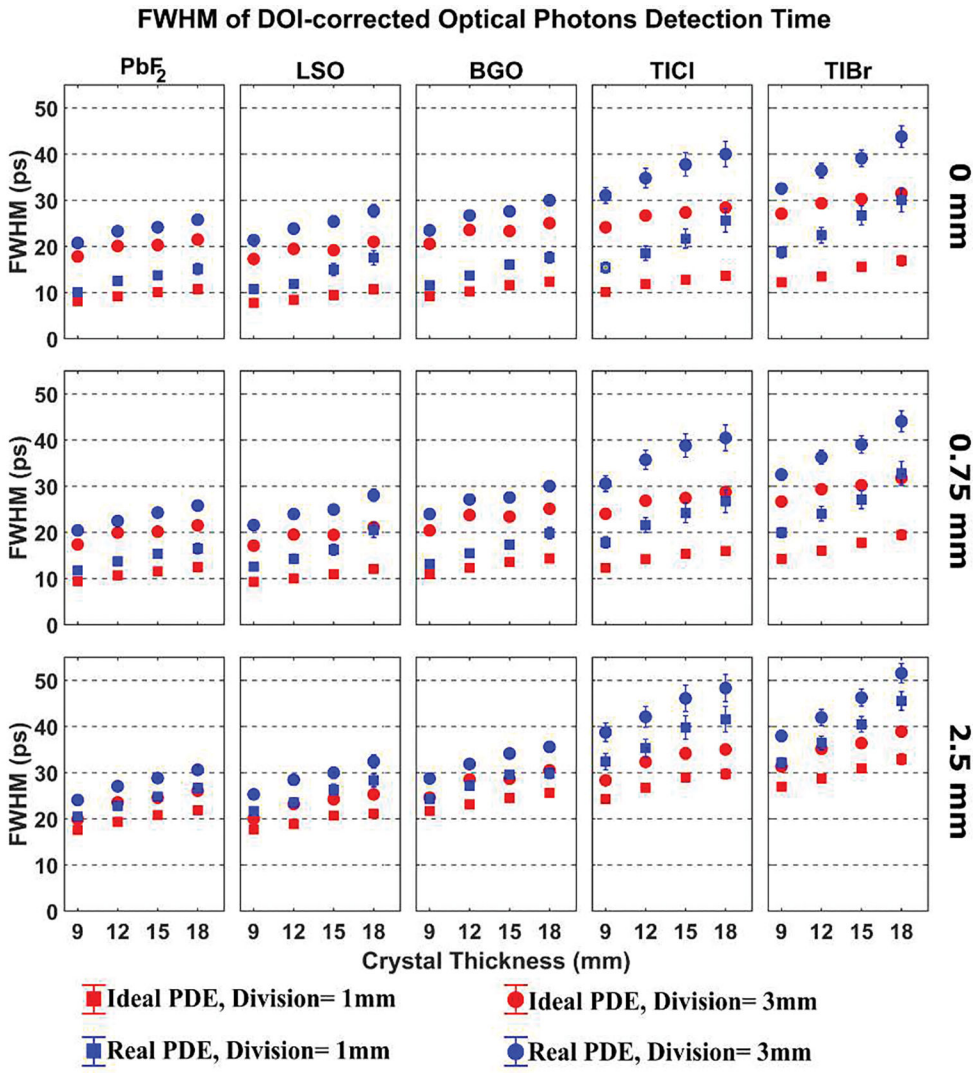

Fig. 7.

Photon time spread characterized by the FWHM of detection time distributions after DOI time walk correction. Top to bottom rows correspond to a different DOI blurring (no blurring, 0.75 mm, and 2.5 mm) representative of an ideal detector, a high-performance detector under development, and the current technology we recently reported, respectively. Four crystal thicknesses were considered for each material and configuration.

Table 1.

Physical properties of LSO, PbF_2, BGO, TlCl, and TlBr

	LSO	**PbF_2**	**BGO**	**TlCl**	**TlBr**
Conductor Type	INS	INS	INS	SC	SC
Refractive Index at 450 nm	1.8	1.8	2.1	2.4	2.6
Cutoff wavelength [nm]	~370	250	320	380	440
Attenuation length at 500 keV [cm]	1.15	0.9	1.09	0.97	0.97
Photofraction at 500 keV [%]	33	46	42	46	43
Effective atomic number, Z_{eff}	66	77	73	77	74
Melting point [°C]	2050	822	1050	431	460

INS in the first row refers to insulator and SC stands for semiconductor.